Enzymatic, urease-mediated mineralization of gellan gum hydrogel with calcium carbonate, magnesium-enriched calcium carbonate and magnesium carbonate for bone regeneration applications

Journal:	*Journal of Tissue Engineering and Regenerative Medicine*
Manuscript ID	TERM-15-0327.R2
Wiley - Manuscript type:	Research Article
Date Submitted by the Author:	n/a
Complete List of Authors:	Douglas, Timothy; University of Gent, Molecular Biotechnology Lapa, Agata; AGH University of Science and Technology, Faculty of Materials Science and Ceramics, Department of Biomaterials Samal, Sangram; Ghent University, Laboratory of General Biochemistry & Physical Pharmacy, Pharmaceutical Declercq, Heidi; Ghent University, Basic Medical Sciencce Schaubroeck, David; Imec, ELIS, Center for Microsystems Technology (CMST) Mendes, Ana; Technical University of Denmark, National Food Institute Van der Voort, Pascal; Ghent University, Department of Inorganic Chemistry Dokupil, Agnieszka; Institute for Chemical Processing of Coal (ICHPW), Plis, Agnieszka; Institute for Chemical Processing of Coal (ICHPW), De Schamphelaere, Karel; Ghent University, Environmental Toxicology Unit (GhEnToxLab) Chronakis, Ioannis; Technical University of Denmark, National Food Institute Pamuła, Elżbieta ; AGH University of Science and Technology, Faculty of Materials Science and Ceramics, Department of Biomaterials Skirtach, Andre; Ghent University, Molecular Biotechnology
Keywords:	hydrogel, gellan gum, mineralization, carbonate, magnesium, composite, enzyme

Enzymatic, urease-mediated mineralization of gellan gum hydrogel with calcium carbonate, magnesium-enriched calcium carbonate and magnesium carbonate for bone regeneration applications

Timothy E.L. Douglas[1]*, Agata Łapa[2‡], Sangram Keshari Samal[3,4], Heidi A. Declercq[5], David Schaubroeck[6], Ana C. Mendes[7], Pascal Van der Voort[8], Agnieszka Dokupil[9], Agnieszka Plis[9], Karel De Schamphelaere[10], Ioannis S. Chronakis[7], Elżbieta Pamuła[2], Andre G. Skirtach[1,4]

[1]Department Molecular Biotechology, Coupure Links 653, 9000 Gent, Belgium, [2]Department of Biomaterials, Faculty of Materials Science and Ceramics, AGH University of Science and Technology, Kraków, Poland, [3]Laboratory of General Biochemistry and Physical Pharmacy, Ghent University, Harelbekestraat 72, 9000 Ghent, Belgium, [4]Centre for Nano- and Biophotonics, Ghent University, Harelbekestraat 72, 9000 Ghent, Belgium, [5]Department of Basic Medical Science – Tissue Engineering Group, Ghent University, De Pintelaan 185 (6B3), 9000 Ghent, Belgium, [6]Center for Microsystems Technology (CMST), imec and Ghent University, Technologiepark 914a, 9052 Ghent, Belgium, [7]Nano-BioScience Research Group, DTU-Food, Technical University of Denmark (DTU), Søltofts Plads, 227, 2800 Kgs. Lyngby, Denmark, [8]Department of Inorganic Chemistry, COMOC, Ghent University, Krijgslaan, 281 S3, 9000, Ghent Belgium, [9]Institute for Chemical Processing of Coal (ICHPW), ul. Zamkowa 1, 41-803 Zabrze, Poland, [10]Laboratory for Environmental and Aquatic Ecology, Environmental Toxicology Unit (GhEnToxLab), Faculty of Bioscience Engineering, Ghent University, Jozef Plateaustraat 22, Gent 9000, Belgium.

*Corresponding Author. Email: Timothy.Douglas@UGent.be

‡Current address : University of Erlangen-Nuremberg Department of Materials Science and Engineering Institute of Biomaterials (WW7) Cauerstr. 6, D-91058 Erlangen, Germany

Keywords: hydrogel, gellan gum, carbonate, mineralization, magnesium, composite, enzyme

Full title: Enzymatic, urease-mediated mineralization of gellan gum hydrogel with calcium and magnesium carbonates for bone regeneration applications

Short title: Hydrogels enzymatically mineralized with Ca/Mg-carbonate

Abstract

Mineralization of hydrogel biomaterials is considered desirable to improve their suitability as materials for bone regeneration. Calcium carbonate ($CaCO_3$) has been successfully applied as a bone regeneration material, but hydrogel-$CaCO_3$ composites have received less attention. Magnesium (Mg) has been used as a component of calcium phosphate biomaterials to stimulate bone-forming cell adhesion and proliferation and bone regeneration *in vivo*, but its effect as a component of carbonate–based biomaterials remains uninvestigated. In this study, gellan gum (GG) hydrogels were mineralized enzymatically with $CaCO_3$, Mg-enriched $CaCO_3$ and magnesium carbonate to generate composite biomaterials for bone regeneration. Hydrogels loaded with the enzyme urease were mineralized by incubation in mineralization media containing urea and different ratios of calcium and magnesium ions. Increasing magnesium concentration decreased mineral crystallinity. At low magnesium concentrations calcite was formed, while at higher concentrations magnesian calcite was formed. Hydromagnesite ($Mg_5(CO_3)_4(OH)_2 \cdot 4H_2O$) formed at high magnesium concentration in the absence of calcium. Amount of mineral formed and compressive strength decreased with increasing magnesium concentration in the mineralization medium. Calcium:magnesium elemental ratio in the mineral formed was higher than in the respective mineralization media. Mineralization of hydrogels with calcite or magnesian calcite promoted adhesion and growth of osteoblast-like cells. Hydrogels mineralized with hydromagnesite displayed higher cytotoxicity. In conclusion, enzymatic mineralization of GG hydrogels with $CaCO_3$ in the

form of calcite successfully reinforced hydrogels and promoted osteoblast-like cell adhesion and growth, but magnesium enrichment had no definite positive effect.

1. Introduction

Gellan gum (GG) is an inexpensive anionic polysaccharide produced biotechnologically using bacteria, from which hydrogels can be formed by crosslinking with divalent ions (Giavasis et al., 2000, Morris et al., 2012). GG hydrogels have been applied as scaffold biomaterials to aid the regeneration of skin (Cerqueira et al., 2014a, Cerqueira et al., 2014b), cartilage and intevertebral discs (Lee et al., 2012, Pimenta et al., 2011, Silva-Correia et al., 2011).

Numerous groups have employed various strategies to enrich hydrogels with a mineral phase to improve their suitability for applications in bone regeneration (for reviews, see (Gkioni et al., 2010, Douglas, 2014). Enrichment with a mineral phase is considered desirable in order to promote bone healing *in vivo* after implantation into a bone defect site (Suzawa et al., 2010, Anderson et al., 2011). The presence of a mineral phase in hydrogels also promotes adhesion, proliferation and osteogenic differentiation of bone-forming cells *in vitro* (Anderson et al., 2011, Bongio et al., 2011, Douglas et al., 2014a, Douglas et al., 2014c, Patel et al., 2010, Phadke et al., 2012). Furthermore, the mineral phase can reinforce the hydrogel mechanically (Douglas et al., 2012, Douglas et al., 2014d, Gyawali et al., 2013, Paxton et al., 2009, Sanginario et al., 2006, Song et al., 2009).

The most commonly used type of mineral to enrich hydrogels is calcium phosphate (CaP), which occurs in different forms such as hydroxyapatite (HA), calcium-deficient apatite, tricalcium phosphate (TCP) and brushite, to name a few. The aforementioned forms of CaP have all been applied as bone regeneration materials. In the case of GG hydrogels, incorporation of a mineral phase has been achieved by addition of inorganic particles (Gantar et al., 2014, Kocen et al., 2014, Douglas et al., 2014b, Canadas et al., 2012, Manda-Guiba et al., 2012) or by enzymatic mineralization with calcium phosphate (CaP) using the enzyme

alkaline phosphatase (ALP), which has not only led to mechanical reinforcement, but also supported osteoblast adhesion and proliferation (Douglas et al., 2014a).

Another inorganic material which has been widely and successfully applied in bone regeneration is calcium carbonate ($CaCO_3$). $CaCO_3$ can occur as amorphous calcium carbonate (ACC) and also as three crystalline polymorphs, namely calcite, found in some sponges and crustaceans, aragonite, present in coral and molluscs, and vaterite, the most thermodynamically unstable form (Sommerdijk and de With, 2008, Muller et al., 2013, Morse et al., 2007). Coral-derived scaffolds, consisting of aragonite, have been reported to have outperformed CaP materials when implanted *in vivo* (Viateau et al., 2013). *In vitro*, coral scaffolds have supported growth and osteogenic differentiation of osteoblasts and mesenchymal stem cells (Tran et al., 2011, Foo et al., 2008, Abramovitch-Gottlib et al., 2006). Nacre, which consists of aragonite crystals embedded in an organic matrix (Corni et al., 2012) has promoted bone formation *in vivo* (Lamghari et al., 1999, Lamghari et al., 2001a, Lamghari et al., 2001b, Liao et al., 2000). Bioactivity, a phenomenon whereby a material binds to bone directly *in vivo*, has been demonstrated for calcite (Fujita et al., 1991). Vaterite has been deposited as a coating on porous polymer scaffolds to stimulate the formation of apatite upon incubation in simulated body fluid (SBF) (Maeda et al., 2007). This suggests that vaterite may display bioactivity *in vivo*. Agarose hydrogels mineralized with $CaCO_3$ in the form of a mixture of calcite and vaterite implanted into rat calvarial defects promoted bone regeneration (Suzawa et al., 2010).

Thus, for the aforementioned physiochemical and biological reasons, it can be expected that enrichment of hydrogels with $CaCO_3$ will improve their suitability as bone regeneration materials. Several enrichment strategies have been reported in literature, including addition of

nacre powder (Flausse et al., 2013), direct formation of $CaCO_3$ during hydrogel formation by delivery of carbonate and calcium ions (Xie et al., 2010), alternate soaking of hydrogels in solutions of calcium and carbonate ions (Ogomi et al., 2003, Suzawa et al., 2010), incubation in solutions of calcium and bicarbonate ions (Munro et al., 2011, Munro and McGrath, 2012), diffusion of CO_2 into hydrogels containing calcium ions (Li and Estroff, 2007, Li et al., 2009) and double-diffusion systems, where calcium and carbonate ions diffuse into hydrogels from different reservoirs (Grassmann and Lobmann, 2003, Grassmann and Lobmann, 2004, Helbig, 2008).

Another, relatively unexplored strategy to generate $CaCO_3$ formation inside hydrogels is the use of enzymes such as urease, which catalyses the conversion of urea and water to form bicarbonate ions and ammonia. Bicarbonate ions can undergo deprotonation to form carbonate ions, which subsequently react with calcium ions to form $CaCO_3$. The generation of ammonia raises the pH of the environment, promoting $CaCO_3$ precipitation. Rauner *et al.* incorporated urease in hydrogels based on hydroxyethyl acrylate and triethylene glycol dimethacrylate or poly(2-ethyl oxazoline), which were subsequently incubated in a mineralization solution containing urea and $CaCl_2$ (Rauner et al., 2014). This resulted in deposition of $CaCO_3$ in the form of aragonite and calcite within the hydrogel network.

Recently, substantial attention has been focused on the enrichment of inorganic, CaP-based materials for bone regeneration with magnesium. Several groups have reported a positive effect of magnesium on osteoblast adhesion, proliferation and differentiation on different CaP-based biomaterials (Boanini et al., 2012, Bracci et al., 2009, Webster et al., 2002, Xue et al., 2008, Yamasaki et al., 2003, Yamasaki et al., 2002, Cai et al., 2010, Landi et al., 2006, Vandrovcova et al., 2015, Zhang et al., 2015). *In vivo*, enrichment of different CaP materials

with magnesium has promoted bone formation, osseointegration and ingrowth of bone (Cabrejos-Azama et al., 2014, Zhao et al., 2012, Landi et al., 2008).

In contrast, magnesium enrichment of $CaCO_3$-based biomaterials for bone regeneration remains unexplored. Magnesium is found in calcite present in mineralized marine organisms including sea urchins and coralline algae (Borzecka-Prokop et al., 2007, Nash et al., 2013, Diaz-Pulido et al., 2014). Naturally occurring calcite can contain up to 30% magnesium (Morse et al., 2007). Synthetic calcites containing up to 39 mol. % magnesium have been produced (Long et al., 2012). In contrast, the maximum magnesium content in magnesium-substituted HA has been reported to be between 5 and 7 mol. % (Ren et al., 2010). Hence, one can expect that $CaCO_3$ biomaterials can be readily enriched with magnesium. Enzymatic mineralization of hydrogels allows straightforward incorporation of other metal ions, e.g. Mg^{2+} into the mineral formed. One merely needs to add such ions to the mineralization medium, as described in previous work (Douglas et al., 2014c).

In this work, GG hydrogels were mineralized enzymatically with calcium and magnesium carbonates using urease. On the basis of previous work on GG hydrogels enzymatically mineralized with CaP (Douglas et al., 2014a) and Mg-enriched CaP (Douglas et al., 2014c) using the enzyme alkaline phosphatase (ALP), it was hypothesized that the presence of carbonate would improve osteoblast-like cell adhesion and proliferation, and that the presence of magnesium would lead to an increase in cell number.

Advantages of using GG over commonly used synthetic hydrogel materials (e.g. poly(ethylene glycol) (PEG), oligo(poly(ethylene glycol) fumarate) (OPF)) are the lack of toxic crosslinkers, and higher mineralizability (Douglas et al., 2012), presumably due to the

affinity of GG for Ca^{2+} ions. In contrast to the widely used natural polysaccharide hydrogel alginate, GG is also crosslinked by Mg^{2+} ions. As one of the aims of this study is to study the effect of magnesium incorporation into carbonate mineral, the use of a hydrogel with affinity for Mg^{2+} ions was considered advantageous.

GG hydrogel samples were loaded with the urease by preincubation in a concentrated urease solution. Hydrogels were subsequently mineralized with calcium and magnesium carbonates by incubation in solutions of urea, a substrate for urease, with five different Ca:Mg concentration ratios. The dependence of the physiochemical and biological properties of the resulting composites on Ca:Mg concentration ratio was evaluated. Physicochemical characterization involved determination of the amount, morphology and nature of mineral formed by attenuated total reflectance Fourier-transform infrared spectroscopy (ATR-FTIR), X-Ray diffraction (XRD), scanning electron microscopy (SEM), inductively coupled plasma optical emission spectroscopy (ICP-OES), thermogravimetric analysis (TGA) and monitoring of the dry mass percentage, i.e. the mass fraction of the hydrogel attributable to mineral and polymer and not to water. Mechanical reinforcement as a result of mineralization was also measured. Biological characterization involved assessment of the cytocompatibility of the composites and their ability to promote the adhesion and proliferation of osteoblast-like cells.

As mentioned above, enrichment of calcium carbonate biomaterials for bone contact with metal ions other than Ca^{2+} (e.g. Mg^{2+}) is not well explored, and neither is enzymatic mineralization of hydrogels with calcium or magnesium carbonates. This study aimed to fill these gaps in the scientific literature and elucidate the physicochemical and biological effects of incorporation of magnesium in carbonate formed in hydrogels.

2. Materials and Methods

2.1 Materials

All materials, including GG (Gelzan™ CM, Product no. G1910, "Low-Acyl", molecular weight 200-300 kD), Urea (U5378), Urease (from Canavalia ensiformis (Jack bean) type III, powder 15.000-50.000 units/g solid, U1500), were obtained from Sigma-Aldrich, unless stated otherwise.

2.2 Production of GG hydrogel samples

GG hydrogel disc samples were fabricated according to a modified form of the method described by Oliveira *et al.* (Oliveira et al., 2010) as described previously (Douglas et al., 2014a, Douglas et al., 2014c). Briefly, 16 ml aqueous 0.875% (w/v) GG solution at 90°C was mixed with 4 ml aqueous 0.15% (w/v) $CaCl_2$ at 90°C, resulting in a GG-$CaCl_2$ solution. After cooling to 50°C, 20 ml GG-$CaCl_2$ solution was cast in glass petri dishes of diameter 10 cm at room temperature and left for 20 min to ensure complete gelation. Final concentrations of GG and $CaCl_2$ were 0.7% (w/v) and 0.03% (w/v), respectively. Hydrogel discs 6 mm in diameter were cut out using a hole punch.

2.3 Loading of hydrogels with enzyme, incubation in mineralization media and subsequent sterilization prior to physicochemical and cell biological characterization

The hydrogel discs were incubated in 5% (w/v) urease solution for 1 h to allow the enzyme to diffuse into the hydrogel. Subsequently, discs were immersed in five different mineralization media at room temperature. These media, denoted hereafter as UA, UB, UC, UD and UE, contained the same concentrations of urea (0.17 M) and different concentrations of $CaCl_2$ and $MgCl_2$. The Ca:Mg concentration ratios in media UA, UB, UC, UD and UE were as follows:

270:0, 202.5:67.5, 135:135, 67.5:202.5 and 0:250, respectively (all values mmol dm^{-3}). An overview is given in Table 1. Mineralization medium was changed every 2 days. After 5 days, the mineralization process was completed. Hydrogel disc samples were placed in Milli-Q water and sterilized by autoclaving at 121°C for 15 minutes (Astell, VWR International, Leuven, Belgium). Unmineralized control samples were prepared by incubating urease-free hydrogel discs in medium UA for 5 days. All physiochemical characterization of hydrogel disc samples was carried out after sterilization by autoclaving, in order to ensure the relevance of the results for later cell biological characterization.

2.4 Determination of extent of mineral formation

The dry mass percentage, i.e. the sample weight percentage attributable to polymer and mineral and not to water, served as a measure of the extent of mineral formation, as in previous publications (Douglas et al., 2012, Douglas et al., 2013, Douglas et al., 2014d). To calculate dry mass percentage, samples were weighed in the wet state immediately after autoclaving, dried at 60°C for 24 h and reweighed in the dry state. Dry mass percentage was defined as: (weight after drying/weight in the wet state before drying)*100%. These measurements were made for all sample groups, n=9.

2.5 Physicochemical and morphological characterization: ATR-FTIR, XRD, SEM, ICP-OES, TGA

Prior to ATR-FTIR, XRD, SEM and ICP-OES analysis, samples were dried as described above. ATR-FTIR was carried out after grinding the dried samples in a ceramic mortar to obtain powders. A JASCO FTIR- 6200 (Tokyo, Japan) equipped with a MIRacle attenuated total reflection (ATR) Crystal Ge (IR penetration 0.66 mm) cell in reflection mode was used.

The samples' transmittance spectra were measured at 32 scans with a resolution of 4 cm^{-1} in the wavelength region 4000-600 cm^{-1}. All the spectra were analyzed with spectrum software.

XRD measurements were performed with a Thermo Scientific™ ARL™ X'TRA Powder Diffractometer set to 40 kV and 30 mA. The slits that were used are: 0.6 and 1 at the source side and 0.6 and 0.2 at the detector side. Scans were made in continuous scan mode over a 2Theta range from 10 to 50 with a step size of 2Theta = 0.02 degrees and a scan rate of 1.2 s/step. A Cu tube was used (Wavelength (nm) 1.540562, Kalpha1: 1.540562, Kalpha2: 1.544390, Kbeta: 1.392218).

SEM was performed using a JEOL JSM-5600 instrument equipped with a secondary electron detector. Samples were sputtered with a thin gold layer (15-20 nm) to make the sample surface conductive.

Prior to determination of elemental content by ICP-OES, a fragment of each dried hydrogel type was weighed on a microbalance to the nearest 0.1 mg and was thermally degraded at 550 °C for 5 h. Residues were dissolved in concentrated HNO_3 (14 mol dm^{-3}), and diluted 20-fold with deionized water to a final concentration of 5% HNO_3 (v/v). The concentrations of calcium and magnesium were determined using ICP-OES after calibration was checked with an independent reference material, for which the deviation is maximum 7.5% (certificate). A procedural blank was analyzed and showed results lower than the quantification limit (0.1 µg/mg for a 10 mg sample). Concentrations of the samples were expressed as µg calcium or magnesium per mg dry weight of the material.

Thermogravimetric analysis (TGA) was carried out using a TG 209 F1 Libra, coupled to a GC Agilent 7890B - MS Agilent 5977A, (NETZSCH-Gerätebau GmbH, Germany). The samples were placed in a crucible made from Al_2O_3. The process of thermal degradation was performed at temperatures between 313 and 1273 K with a heating rate of 10 K/min under flow of argon (25 ml/min) as a purge gas. The weight of the samples was in the range 7.0-10.0 mg and weight was measured with an accuracy of ± 0.1 mg. The results obtained allowed the assessment of the mass losses during the procedure as well as the initial and final temperatures of each stage of the degradation process. Measurements were performed in triplicate for all sample groups.

2.6 Mechanical testing

Mechanical characterization: A Texture Analyzer TA.XTPlus Texture Analyzer (Stable Micro Systems, UK), with a 5 kg load cell was used for the mechanical characterization of the hydrogel samples. The resistance of the samples to the compression made by a metallic cylinder probe with a diameter of 15 mm was recorded. The pre-test speed was set at 2.00 mm/s, the test speed at 1.00 mm/s, with a compression of the sample to 80% of its original height, and the post-test speed at 1.00 mm/s. The experiments were carried out at room temperature. The analyses were performed on three replicate samples.

2.7 Characterization of osteoblast-like cell attachment and growth

2.7.1 Cell culture and seeding on hydrogel samples

MC3T3-E1 (subclone 14) cells (ATCC) were cultured in α-MEM GlutaMAX-1™ medium (Gibco Invitrogen) supplemented with 10% foetal calf serum (FCS, Gibco Invitrogen), P/S (10 U/ml penicillin, 10mg/ml streptomycin, Gibco Invitrogen) and 100 mM sodium-pyruvate

(Gibco Invitrogen). Cells were cultured at 37 °C in a humidified atmosphere containing 5% CO_2. The medium was changed 2 times a week.

Hydrogel samples were sterilized by autoclaving at 1 bar during 20 minutes (Astell, VWR International, Leuven, Belgium).

For the cell adhesion assay, MC3T3 cells were seeded at a density of 40000 cells/0.5 ml culture medium/hydrogel and evaluated after 1 day. For the cell proliferation assay, MC3T3 cells were seeded at a density of 20000 cells/0.5 ml culture medium/hydrogel and evaluated after 1 and 7 days. Cells cultured on tissue culture polystyrene (TCPS) were taken as a positive control.

2.7.2 Fluorescence and Conforcal Laser Scanning Microscopy (CLSM)

To visualize cell attachment, morphology and distribution on the hydrogels, the cell cultures were evaluated using inverted fluorescence microscopy and confocal laser scanning microscopy.

A live/dead staining (Calcein AM/propidium iodide) was performed to evaluate cell viability. After rinsing, the supernatant was replaced by 1 ml PBS solution supplemented with 2 µl (1 mg/ml) calcein AM (Anaspec, USA) and 2 µl (1 mg/ml) propidium iodide (Sigma). Cultures were incubated for 10 min at room temperature and washed twice with PBS solution. Cells were evaluated by fluorescence microscopy (Type U-RFL-T, XCellence Pro software, Olympus, Aartselaar, Belgium) and confocal laser scanning microscopy (CLSM) (Nikon D-Eclipse C1 inverted microscope with a 60X water immersion objective, Japan, NIS-Elements Confocal software). Evaluations were done 1 and 7 days post-seeding.

2.7.3 MTT assay

The colorimetric MTT assay, using a 3-(4, 5-dimethyldiazol-2-yl)-2, 5-diphenyltetrazolium bromide (MTT, Merck Promega) was performed to quantify cell viability and proliferation on the hydrogels.

The tetrazolium component is reduced in living cells by mitochondrial dehydrogenase enzymes into a water-insoluble purple formazan product, which can be solubilized by addition of lysis buffer and measured using spectrophotometry.

The cell culture medium was replaced by 0.5 ml (0.5 mg/ml) MTT reagent and cells were incubated for 4 h at 37°C. After removal of the MTT reagent, 0.5 ml lysis buffer (1% Triton X-100 in isopropanol/0.04N HCl) was added and incubated for 30 min at 37°C on a gyratory shaker (70 rpm). 200 µl of the dissolved formazan solution was transferred into a 96-well plate and measured spectrophotometrically at 580 nm (Universal microplate reader EL 800, Biotek Instruments).

Triplicate measurements were performed 1 and 7 days post-seeding. The amount of viable attached cells was calculated as a percentage of control cultures after 1 and 7 days.

2.8 Statistical Analysis

Student's T-test was applied to determine statistical significance using Excel software. A two-tailed unpaired t-test with 95% confidence interval was considered statistically significant if $P < 0.05$ (*), $P < 0.01$ (**) and $P < 0.001$ (***).

3. Results

3.1 Physicochemical characterization of mineral formed: FTIR, XRD and SEM

FTIR spectra of mineralized hydrogel samples are displayed in Figure 1. In samples from group UA, UB, UC and UD mineral which was formed is calcite. The bands at 712 and 871

cm^{-1}, corresponding to υ_4 and υ_2 symmetric and antisymmetric bending of carbonate groups, respectively, are typical for calcite, as is the broad band at approximately 1400 cm^{-1}, corresponding to υ_3 antisymmetric stretching (Sato and Matsuda, 1969, Andersen and Brecevic, 1991, Xyla and Koutsoukos, 1989). The sample group UE displayed a markedly different absorption spectra which indicated the presence of the magnesium carbonate hydromagnesite ($Mg_5(CO_3)_4(OH)_2 \cdot 4H_2O$). The bands at 714, 744 and 792 cm^{-1}, corresponding to υ_4 and υ_2 symmetric and antisymmetric bending of carbonate groups, the double band at 1478 and 1416 cm^{-1}, corresponding to υ_3 antisymmetric stretching of carbonate groups, and the shoulder at 1646 cm^{-1}, corresponding to the water bending vibration of strongly hydrogen bonded water molecules, are all indicative of hydromagnesite (White, 1971, Frost, 2011). The major characteristic bands for GG at approximately 1600 and 1030 cm^{-1}, observed in previous work (Douglas et al., 2014a, Douglas et al., 2014c, Douglas et al., 2015), were not observed in any sample group, suggesting that the proportion of mineral present in the samples was much higher than the proportion of GG present.

XRD analysis also revealed differences between the sample groups UA, UB, UC, UD and UE. The mineral formed in samples groups UA and UB displayed peaks at 2theta values of 23.2, 29.5, 36.1, 39.5, 43.3, 47.7 and 48.6 which are characteristic for calcite (Rahman et al., 2013) (see Supplementary Figure S1). In samples incubated in UC and UD, the peak at 29.5, characteristic of the (104) plane of calcite, shifted to 29.8, which is characteristic of magnesian calcite (Diaz-Pulido et al., 2014). The intensity of the peaks decreased in the order UA > UB > UC > UD. Furthermore, in samples incubated in UD, small peaks were present at 26.3 and 45.9 which may indicate aragonite (see Supplementary Figure S1). Samples incubated in UE exhibited peaks at 2theta values of approximately 14.0, 15.4, 30.9, 35.9 and 42.0 which are consistent with the presence of hydromagnesite (Hanchen et al., 2008, Suzuki

et al., 2012) (see Supplementary Figure S1). The aforementioned peaks were much smaller and less sharp than those in the diffraction patterns of the other samples, suggesting markedly greater amorphicity. The major characteristic peak for GG at a 2theta value of approximately 20, observed in previous work (Douglas et al., 2014a), was not observed in any sample group, suggesting that the proportion of mineral present in the samples was much higher than the proportion of GG present.

SEM images of mineral deposits formed in sample groups UA, UB, UC, UD and UE are shown in Figure 3. SEM analysis revealed the presence of cube-like deposits characteristic of calcite in sample groups UA and UB (Figure 3 i-iv), Mineral formed in sample group UC was in the form of ellipsoidal deposits exhibiting a porous surface (Figure 3 v-vii). Mineral in sample group UD comprised cuboid-like deposits covered with undefined spherical deposits (Figure 3 viii-ix). Plate-like deposits characteristic of hydromagnesite were observed in sample group UE, together with numerous undefined spherical deposits (Figure 3 x-xii). From previous work, unmineralized GG samples are known to be smooth and devoid of deposits (Douglas et al., 2014a, Douglas et al., 2014c).

3.2 Influence of mineralization medium on extent of mineralization, elemental composition of mineral formed and thermal degradation

The dry mass percentages of sample groups UA, UB, UC, UD and UE are shown in Figure 4. Generally speaking, values decreased with increasing magnesium concentration in the mineralization medium. The values for UA samples were markedly higher than those for UD and UE samples. From previous work (Douglas et al., 2014a, Douglas et al., 2014c) it is known that the values for unmineralized GG samples range between approximately 0 and 2 %. This is markedly less than the values observed for the sample groups in this study.

Elemental amounts of calcium and magnesium in sample groups UA, UB, UC, UD and UE are presented in Table 2. Calcium was preferentially incorporated into mineral formed. The molar percentage of elemental magnesium (Mg/(Mg+Ca)*100%) present in mineral formed in group UA was negligible. This value increased to 3.3 mol. % for group UB and rose further to 9.8 mol. % for group UC and 17.9% for group UD. Group UE contained almost exclusively magnesium (>98%). The small amount of calcium detected can be ascribed to the calcium used to crosslink GG polymer during hydrogel production.

TGA results showing dependence of thermal degradation on temperature are shown in Figure 5. In sample group UA, the first noteworthy mass decrease occurred between approximately 850 K and 1050 K. This corresponds to the decomposition of calcite to CaO and CO_2 (Frost et al., 2009). In previous work on GG hydrogels mineralized with CaP, a mass decrease between approximately 525 K and 725 K was seen, corresponding to degradation of GG polymer (Douglas et al., 2014a). This decrease was practically imperceptible in group UA, suggesting that the amount of organic component was much lower than the amount of inorganic component. The results for group UB were similar, however small mass decreases were observed from approximately 300 K to 500 K and from approximately 525 K to 725 K. The first decrease may be ascribed to evaporation of loosely bound water. The second decrease can be ascribed to degradation of the polymer GG component of the mineralized hydrogels, respectively. In group UC, the aforementioned mass decreases were more pronounced. Furthermore, a gradual decrease after 725 K was observed, which may be due to release of CO_2, which has been reported previously for ACC (Ihli et al., 2013, Raz et al., 2002). In group UD, these mass decreases were even more pronounced. Furthermore, the main mass decrease occurred at a lower temperature and was completed at approximately 1000 K. This

suggested the presence of higher amounts of water and organic component, as well as increased amorphicity. The thermal decomposition profile of UE was markedly different, suggesting the presence of another mineral phase. A larger mass decrease was seen in the 300-450 K range, suggesting that more water was bound. The most notable differences to other sample groups were the markedly larger mass decrease in the 450-600 K temperature ranges and the fact that the main mass decrease occurred in a markedly lower temperature range, namely 625-725 K. These mass decreases are characteristic for hydromagnesite and correspond to release of the water molecules, i.e. $Mg_5(CO_3)_4(OH)_2 \cdot 4H_2O \rightarrow Mg_5(CO_3)_4(OH)_2$, and decomposition of $Mg_5(CO_3)_4(OH)_2$ into MgO, CO_2 and H_2O, respectively (Hollingbery and Hull, 2010). From TGA measurements of unmineralized GG samples in previous work (Douglas et al., 2014a, Douglas et al., 2014c), it is known that the mass percentage remaining at 1073 K is approximately 10-15%, i.e. markedly lower than the values obtained for the sample groups UA-UE in this study.

3.3 Effect of mineralization on hydrogel mechanical properties

The results of compressive testing are shown in Figure 6. From UA to UD, the values of compression force decreased markedly. The values for UE samples were twice as high as those for UD but still lower than those for UC. Unmineralized GG samples were markedly weaker than all other sample groups.

3.4 Cell biological characterization with MC3T3-E1 osteoblast-like cells

Fluorescence and confocal laser scanning microscopy images of MC3T3-E1 cells on sample groups UA, UB, UC, UD, UE and unmineralized GG hydrogels after 1 and 7 days are presented in Figure 7. After 1 day, viable (green) cells were observed on the surface of all sample groups (Figure 7 i, iii, v, vii, xi) except for UE. Mainly dead (red) cells with a round

morphology were observed on hydrogel UE (Figure 7 ix) . The cells on the hydrogels UA, UB, UC and UD have a spread morphology (Figure 7 inserts), demonstrating the good adhesion on the modified hydrogels. In contrast, cells observed on the unmineralized GG hydrogels have a round morphology, typical for non-adherent cells (Figure 7 xi insert). After 7 days, calcein AM stained cells were evaluated by CLSM. The same trend was observed as after 1 day. Cells on the hydrogels UA, UB, UC and UD showed viable cells with a well spread morphology (Figure 7 ii, iv, vi, viii). On the hydrogels UE and unmineralized GG, only a few viable rounded cells (Figure 7 x, xii), typical for non-adherent cells, were observed.

These qualitative results of the live/dead staining were confirmed by the quantitative MTT assay as shown in Figure 8. After seeding cells at a high concentration (cell adhesion assay), a comparable amount of viable cells (varying from 28.4% to 42. %) adhered on the hydrogels UA, UB, UC and UD in contrast to the hydrogels UE (3 %) and GG (5.9%). In the proliferation assay, the same trend could be observed after 1 day. After 7 days, the amount of viable and attached cells on hydrogels UA, UC and UD had increased 3-to-6 fold, except for UB where the cells only showed a 1.6-fold increase. The amount of viable cells on UE and GG showed only a minor increase compared to day 1.

4. Discussion

The goals of this study were i) the enzymatic mineralization of GG hydrogels with carbonate mineral to create hydrogel-mineral composite biomaterials and ii) investigation of the effect of mineralization medium, in particular magnesium concentration, on the physiochemical and

biological characteristics of the composites. Magnesium concentration in the mineralization medium increased in the order UA > UB > UC > UD > UE.

4.1. Physicochemical characterization

Mineral formation in all sample groups was demonstrated directly by visualization of mineral deposits by SEM (Figure 3), detection of bands characteristic for carbonate groups by FTIR (Figure 1) and peaks characteristic for calcite (UA, UB), magnesian calcite (UC, UD) or hydromagnesite (UE) by XRD (Figure 2). Further indirect proof was provided by the increases in dry mass percentage (Figure 4), detection of elemental Ca and Mg by ICP-OES (Table 2), monitoring of thermal degradation by TGA (Figure 5) and increases in resistance to compressive deformation in comparison to unmineralized GG hydrogels (Figure 6).

Magnesium concentration in the mineralization medium increased in the order UA > UB > UC > UD > UE. Increasing magnesium concentration led to a reduction in mineral formed, as shown by the changes in dry mass percentage, i.e. UA > UD, UE (Figure 4), the decrease in mass of elemental calcium and magnesium detected, i.e. UA > UD, >> UE (Table I), the decrease in mechanical properties in the order UA > UB > UC > UD < UE (Figure 6), and the increased mass decrease between approximately 525 K and 725 K observed using TGA (Figure 5). ICP-OES results (Table 2) demonstrated that magnesium content rose with increasing ratio of calcium to magnesium in the mineralization media. In addition, the ratio of calcium to magnesium in carbonate formed in groups UA, UB, UC and UD was much higher than in the respective mineralization media. This is in agreement with studies on the effect of Mg/Ca elemental ratio in seawater on the incorporation of magnesium into marine invertebrate exoskeletons and non-skeletal precipitation (Ries, 2004, Stanley et al., 2002). This preferential incorporation of calcium has also been observed for CaP and can be explained by the following theory proposed by Martin and Brown (Martin and Brown, 1997).

Magnesium ions in solution are more hydrated than calcium ions and undergo dehydration more slowly. As a result, magnesium ions can adsorb to $CaCO_3$ but do not dehydrate sufficiently fast to be included in the carbonate mineral, and thus remain on the surface. From our data, it is unclear to how much magnesium is present on the surface of carbonate deposits and how much is incorporated into the bulk. On the basis of XRD data (Figure 2), the mineral formed in sample groups UC and UD appeared to be magnesian calcite. Raz et al. postulated that magnesian calcite forms via an amorphous precursor phase (Raz et al., 2000). The authors suggested that hydrated magnesium ions can be more easily incorporated in the amorphous precursor phase, which increases their chance of incorporation into the final crystalline magnesian calcite phase. It is possible that the presence of magnesium helps to stabilize the amorphous phase. Indeed, magnesium has been reported to "poison" calcite formation (Folk, 1974), presumably by binding to the surface of calcite nuclei and inhibiting further crystal growth due to its residual water of hydration.

The mass decreases ascribed to water measured using TGA (Figure 5) increased in the order UA > UB > UC > UD > UE. This may be due to an increase in amorphicity, with the associated increases in incorporation of partially hydrated magnesium ions. Further evidence of increasing amorphicity in the order UA > UB > UC > UD > UE is provided by the increasing occurrence of undefined non-crystalline mineral deposits by SEM (Figure 3). The decrease in the intensity of XRD peaks (Figure 2) might also be indicative in increasing amorphicity, but might also indicate a range of Mg substitution, less well crystallized, defects in the crystal lattice that stretches the cell size.

The decreasing crystallinity of the mineral formed, and thus the increasing solubility, in the order UA > UB > UC > UD > UE, partially explains why mineral formation was lowest in groups UD and UE (Figure 4, Table 2).

Mechanical testing results (Figure 6) showed that resistance to compressive loading, which decreased in the order UA > UB > UC > UD. Mechanical resistance of the samples seems to decrease with the decrease of mineral content formed. Such data is in agreement with the decrease in dry mass percentage (Figure 4). Nevertheless, the mechanical force necessary to compress sample UE by 80% of its original height was shown to be superior to the value for sample UD. The reasons for this are unclear. All sample groups UA-UE showed enhanced mechanical resistance compared to the unmineralized GG controls. This is evidence of the potential of the mineralization method applied in this study to raise mechanical strength. In previous studies, mineralization of GG hydrogels with CaP led to marked increases in resistance to compressive loading (Douglas et al., 2014a, Douglas et al., 2014b, Douglas et al., 2014c). In this study, all samples were sterilized by autoclaving before mineralization, as sterility is a pre-requisite for cell biological characterization. Previous studies have shown that autoclaving of mineralized hydrogels decreases their resistance to compressive loading (Douglas et al., 2014a).

4.2 Cell biological characterization

The Live/dead staining results suggested that sample groups UA, UB, UC and UD supported cell adhesion and growth. (Figure 7). In a previous publication on GG hydrogels enzymatically mineralized with CaP (Douglas et al., 2014a), MC3T3-E1 cell adhesion rose markedly as a result of hydrogel mineralization with CaP. In another previous publication, ALP-enriched GG hydrogels were mineralized with five different mineralization solutions of varying Ca:Mg molar ratios in order to assess the effect of magnesium on the physiochemical and biological properties of the resulting composites (Douglas et al., 2014c). Incorporation of magnesium into CaP mineral formed in gellan gum hydrogels led to enhanced osteoblast-like cell adhesion and proliferation after 1 day and 11 days. This magnesium-induced effect was

independent of the crystallinity of the CaP formed (calcium-deficient apatite or amorphous CaP). However, in this study, the incorporation of magnesium into carbonate mineral did not lead to any obvious positive effect on cell adhesion and proliferation after 1 day or 7 days (Figures 7 & 8). The biological effects of magnesium as a component of calcium carbonate may differ from its effects as a component of CaP materials. In the absence of further data, such discussion must remain speculative.

4.3 Outlook

Cell biological characterization in this study focused on MC3T3-E1 cell adhesion and proliferation on two-dimensional surfaces. Further work will focus on the differentiation of MC3T3-E1 cells on the sample groups. Furthermore, since cells are known to behave differently in 2D and 3D environments, modification of hydrogel 3D internal architecture will be a further point of consideration. Such experiments will pave the way for the implantation of the mineralized hydrogels in bone defects, as described by other authors (Suzawa et al., 2010).

5. Conclusion

GG hydrogels were enzymatically mineralized with an inorganic phase consisting of calcium, magnesium and carbonates. It was observed that calcium was incorporated into carbonate mineral formed to a greater extent than magnesium. Increasing the amount of magnesium in the mineralization medium led to a reduction in the amount and crystallinity of the carbonate mineral formed. By increasing magnesium concentration, the type of the detected crystalline carbonate phase changed from calcite in sample groups UA and UB, to magnesian calcite in

sample groups UC and UD, to hydromagnesite in sample group UE. Cellular adhesion and proliferation was far superior on UA, UB, UC and UD compared to GG. The presence of magnesium in mineral formed did not clearly promote adhesion or proliferation. Sample group UE, containing only magnesium carbonate, showed higher cytotoxicity after 1 and 7 days.

6. Acknowledgement

Timothy E.L. Douglas and Andre Skirtach acknowledge the Research Foundation Flanders (FWO) for support in the framework of a postdoctoral fellowship. Joanna Aernoudt, Tom Planckaert, Nancy De Saeyer and Emmy Peuquer are thanked for excellent technical assistance. BOF (Bijzonder Onzderzoeksfonds) of Ghent University is thanked for support.

7. Conflict of Interest, Ethical Approval and Original Publication Statements

The authors have no conflict of interest. No ethical approval was required for this study. No part of this work has been previously published or submitted for publication elsewhere.

8. Tables

Mineralization medium	*Concentration*		
	$CaCl_2$	*$MgCl_2$*	*urea*
	(mol dm^{-3})	*(mol dm^{-3})*	*(mol dm^{-3})*
UA	0.27	0	0.17
UB	0.0675	0.2025	0.17
UC	0.135	0.135	0.17
UD	0.2025	0.0675	0.17
UE	0.025	0.27	0.17

Table 1. Mineralization media used in this study.

Sample group	*µg element/mg sample*		*µmol element/mg sample*		*Molar % of Mg (Mg/(Mg+Ca))*100 in sample*
	Ca	*Mg*	*Ca*	*Mg*	
UA	373	<0.1	9.3	<0.005	<0.05
UB	367	7.7	9.2	0.3	3.3
UC	333	22	8.3	0.9	9.8
UD	301	40	7.5	1.6	17.9
UE	5.4	227	0.1	9.3	98.6

Table 2. ICP-OES determination of mass elemental calcium and magnesium per unit mass of dried GG hydrogels preincubated in 50 mg/ml urease and subsequently incubated for 5 days in mineralization media UA, UB, UC, UD or UE.

9. Figure Captions

Figure 1. FTIR spectra in the wavelength range 600-4000 cm^{-1} of GG hydrogels preincubated in 50 mg/ml urease and subsequently incubated for 5 days in mineralization media UA, UB, UC, UD and UE. Bands characteristic for calcite in sample groups UA, UB, UC and UD are

visible at 1400, 871 and 712 cm^{-1}. Bands characteristic for hydromagnesite in sample group UE are visible at 1478, 1416, 792, 744 and 714 cm^{-1}. A shoulder characteristic for hydromagnesite is visible at 1646 cm^{-1}.

Figure 2. XRD diffractograms of GG hydrogels preincubated in 50 mg/ml urease and subsequently incubated for 5 days in mineralization media UA, UB, UC, UD or UE. C: calcite; MC: magnesian calcite; A: aragonite; HM: hydromagnesite.

Figure 3. SEM micrographs of GG hydrogels preincubated in 50 mg/ml urease and subsequently incubated for 5 days in mineralization media UA, UB, UC, UD or UE. i, ii: UA; iii, iv: UB; v, vi, vii: UC; viii, ix: UD; x, xi, xii: UE. Scale bars: i: 10 µm; ii: 5 µm; iii: 10 µm; iv: 5 µm; v: 50 µm; vi: 5 µm; vii: 1 µm; viii: 10 µm; ix: 5 µm; x: 50 µm; xi: 10 µm; xii: 5 µm. The scale bars are indicated on each figure.

Figure 4. Dry mass percentage of GG hydrogels preincubated in 50 mg/ml urease and subsequently incubated for 5 days in mineralization media UA, UB, UC, UD or UE. Error bars show standard deviation.

Figure 5. Thermogravimetric analysis of GG hydrogels preincubated in 50 mg/ml urease and subsequently incubated for 5 days in mineralization media UA, UB, UC, UD or UE. Representative graphs showing residual mass percentage (TG) and rate of change of TG (DTG) are shown for each sample group. Bottom right: residual mass percentage after heating to 1273 K. Error bars show standard deviations. No statistically significant differences were observed.

Figure 6. Compressive testing of GG hydrogels preincubated in 50 mg/ml urease and subsequently incubated for 5 days in mineralization media UA, UB, UC, UD or UE. y-axis: force required to compress samples by 80%. Error bars show standard deviation.

Figure 7. Fluorescence and Confocal Laser Scanning microscopy images of MC3T3-E1 osteoblast-like cells cultivated for 1 day and 7 days on GG hydrogels preincubated in 50 mg/ml urease and subsequently incubated for 5 days in mineralization media UA, UB, UC, UD or UE. Fluorescence microscopy (i, iii, v, vii, ix, xi and inserts) evaluation of cells seeded at a high concentration (cell adhesion test) on GG hydrogels after 1 day. Confocal laser scanning microscopy (ii, iv, vi, viii, x, xii) evaluation of cells seeded at a low concentration (cell proliferation test) on GG hydrogels after 7 days.

i, ii: UA, 1 and 7 days respectively; iii, iv: UB, 1 and 7 days respectively; v, vi: UC: 1 and 7 days respectively; vii, viii: UD: 1 and 7 days respectively; ix, x: UE: 1 and 7 days respectively; xi, xii: GG: 1 and 7 days respectively.

Figure 8. Percentage of viable attached cells on GG hydrogels preincubated in 50 mg/ml urease and subsequently incubated for 5 days in mineralization media UA, UB, UC, UD or UE. Cells were seeded and evaluated after 1 day (cell adhesion) respectively 1 and 7 days (cell proliferation). The amount of viable cells was quantified using the MTT assay by calculating relative to the control (tissue culture polystyrene) of day 1 (cell adhesion) or day 7 (cell proliferation).

Supplementary Figure 1: Standard XRD diffraction patterns for aragonite (top), calcite (middle) and hydromagnesite (bottom).

10. References

ABRAMOVITCH-GOTTLIB, L., GERESH, S. & VAGO, R. (2006) Biofabricated marine hydrozoan: a bioactive crystalline material promoting ossification of mesenchymal stem cells. *Tissue Eng,* 12**,** 729-39.

ANDERSEN, F. A. & BRECEVIC, L. (1991) Infrared-Spectra of Amorphous and Crystalline Calcium-Carbonate. *Acta Chemica Scandinavica,* 45**,** 1018-1024.

ANDERSON, J. M., PATTERSON, J. L., VINES, J. B., JAVED, A., GILBERT, S. R. & JUN, H. W. (2011) Biphasic peptide amphiphile nanomatrix embedded with hydroxyapatite nanoparticles for stimulated osteoinductive response. *ACS Nano,* 5**,** 9463-79.

BOANINI, E., TORRICELLI, P., FINI, M., SIMA, F., SERBAN, N., MIHAILESCU, I. N. & BIGI, A. (2012) Magnesium and strontium doped octacalcium phosphate thin films by matrix assisted pulsed laser evaporation. *J Inorg Biochem,* 107**,** 65-72.

BONGIO, M., VAN DEN BEUCKEN, J. J., NEJADNIK, M. R., LEEUWENBURGH, S. C., KINARD, L. A., KASPER, F. K., MIKOS, A. G. & JANSEN, J. A. (2011) Biomimetic modification of synthetic hydrogels by incorporation of adhesive peptides and calcium phosphate nanoparticles: in vitro evaluation of cell behavior. *Eur Cell Mater,* 22**,** 359-76.

BORZECKA-PROKOP, B., WESELUCHA-BIRCZYNSKA, A. & KOSZOWSKA, E. (2007) MicroRaman, PXRD, EDS and microscopic investigation of magnesium calcite biomineral phases. The case of sea urchin biominerals. *Journal of Molecular Structure,* 828**,** 80-90.

BRACCI, B., TORRICELLI, P., PANZAVOLTA, S., BOANINI, E., GIARDINO, R. & BIGI, A. (2009) Effect of Mg(2+), Sr(2+), and Mn(2+) on the chemico-physical and in vitro biological properties of calcium phosphate biomimetic coatings. *J Inorg Biochem,* 103**,** 1666-74.

CABREJOS-AZAMA, J., ALKHRAISAT, M. H., RUEDA, C., TORRES, J., BLANCO, L. & LOPEZ-CABARCOS, E. (2014) Magnesium substitution in brushite cements for enhanced bone tissue regeneration. *Materials Science & Engineering C-Materials for Biological Applications,* 43**,** 403-410.

CAI, Y. L., ZHANG, J. J., ZHANG, S., VENKATRAMAN, S. S., ZENG, X. T., DU, H. J. & MONDAL, D. (2010) Osteoblastic cell response on fluoridated hydroxyapatite coatings: the effect of magnesium incorporation. *Biomed Mater,* 5**,** 054114.

CANADAS, R., PEREIRA, D. R., SILVA-CORREIA, J., MARQUES, A. P., OLIVEIRA, J. M. & REIS, R. L. (2012) Novel bilayered Gellan gum/Gellan gum-hydroxyapatite scaffolds for osteochondral tissue engineering applications. *J Tissue Eng Regen Med,* 6**,** 16-16.

CERQUEIRA, M. T., DA SILVA, L. P., SANTOS, T. C., PIRRACO, R. P., CORRELO, V. M., MARQUES, A. P. & REIS, R. L. (2014a) Human Skin Cell Fractions Fail to Self-Organize Within a Gellan Gum/Hyaluronic Acid Matrix but Positively Influence Early Wound Healing. *Tissue Eng Part A,* 20**,** 1369-1378.

CERQUEIRA, M. T., DA SILVA, L. P., SANTOS, T. C., PIRRACO, R. P., CORRELO, V. M., REIS, R. L. & MARQUES, A. P. (2014b) Gellan Gum-Hyaluronic Acid Spongy-like Hydrogels and Cells from Adipose Tissue Synergize Promoting Neoskin Vascularization. *Acs Appl Mater Inter,* 6**,** 19668-19679.

CORNI, I., HARVEY, T. J., WHARTON, J. A., STOKES, K. R., WALSH, F. C. & WOOD, R. J. K. (2012) A review of experimental techniques to produce a nacre-like structure. *Bioinspiration & Biomimetics,* 7.

DIAZ-PULIDO, G., NASH, M. C., ANTHONY, K. R. N., BENDER, D., OPDYKE, B. N., REYES-NIVIA, C. & TROITZSCH, U. (2014) Greenhouse conditions induce mineralogical changes and dolomite accumulation in coralline algae on tropical reefs. *Nature Communications,* 5.

DOUGLAS, T., WLODARCZYK, M., PAMULA, E., DECLERCQ, H., DE MULDER, E., BUCKO, M., BALCAEN, L., VANHAECKE, F., CORNELISSEN, R., DUBRUEL, P., JANSEN, J. & LEEUWENBURGH, S. (2014a) Enzymatic mineralization of gellan gum hydrogel for bone tissue-engineering applications and its enhancement by polydopamine. *J Tissue Eng Regen Med,* 8**,** 906–918.

DOUGLAS, T. E., MESSERSMITH, P. B., CHASAN, S., MIKOS, A. G., DE MULDER, E. L., DICKSON, G., SCHAUBROECK, D., BALCAEN, L., VANHAECKE, F., DUBRUEL, P., JANSEN, J. A. & LEEUWENBURGH, S. C. (2012) Enzymatic mineralization of hydrogels for bone tissue engineering by incorporation of alkaline phosphatase. *Macromol Biosci,* 12**,** 1077-89.

DOUGLAS, T. E., PIWOWARCZYK, W., PAMULA, E., LISKOVA, J., SCHAUBROECK, D., LEEUWENBURGH, S. C., BRACKMAN, G., BALCAEN, L., DETSCH, R., DECLERCQ, H., CHOLEWA-KOWALSKA, K., DOKUPIL, A., CUIJPERS, V. M., VANHAECKE, F., CORNELISSEN, R., COENYE, T., BOCCACCINI, A. R. & DUBRUEL, P. (2014b) Injectable self-gelling composites for bone tissue engineering based on gellan gum hydrogel enriched with different bioglasses. *Biomed Mater,* 9**,** 045014.

DOUGLAS, T. E., SKWARCZYNSKA, A., MODRZEJEWSKA, Z., BALCAEN, L., SCHAUBROECK, D., LYCKE, S., VANHAECKE, F., VANDENABEELE, P., DUBRUEL, P., JANSEN, J. A. & LEEUWENBURGH, S. C. (2013) Acceleration of gelation and promotion of mineralization of chitosan hydrogels by alkaline phosphatase. *Int J Biol Macromol,* 56C**,** 122-132.

DOUGLAS, T. E. L. (2014) Apatite Enrichment of Hydrogel Biomaterials for Bone Regeneration. IN IAFISCO, M. & DELGADO-LOPEZ, J. M. (Eds.) *Apatite: Synthesis, Structural Characterization and Biomedical Applications.* New York, Nova Publishers.

DOUGLAS, T. E. L., KRAWCZYK, G., PAMULA, E., DECLERCQ, H., SCHAUBROECK, D., BUCKO, M. M., BALCAEN, L., VAN DER VOORT, P., BLIZNUK, V., VAN DER VREKEN, N. M., VANHAECKE, F., DASH, M., DETSCH, R., BOCCACCINI, A. R., CORNELISSEN, R. & DUBRUEL, P. (2014c) Generation of composites for bone tissue engineering applications consisting of gellan gum hydrogels mineralized with calcium and magnesium phosphate phases by enzymatic means. *J Tissue Eng Regen Med*.

DOUGLAS, T. E. L., PIEGAT, A., DECLERCQ, H. A., SCHAUBROECK, D., BALCAEN, L., BLIZNUK, V., DE MEYER, B., VANHAECKE, F., CORNELISSEN, M., EL FRAY, M. & DUBRUEL, P. (2014d) Composites of polyvinyl alcohol (PVA) Hydrogel and calcium and magnesium phosphate formed by enzymatic functionalization. *Materials Letters,* 137**,** 62-67.

DOUGLAS, T. E. L., PILARZ, M., LOPEZ-HEREDIA, M., BRACKMAN, G., SCHAUBROECK, D., BALCAEN, L., BLIZNUK, V., DUBRUEL, P., KNABE-DUCHEYNE, C., VANHAECKE, F., COENYE, T. & PAMULA, E. (2015) Composites of gellan gum hydrogel enzymatically mineralized with calcium–zinc phosphate for bone regeneration with antibacterial activity. *J Tiss Eng Regen Med,* EPub 15.7.2015.

FLAUSSE, A., HENRIONNET, C., DOSSOT, M., DUMAS, D., HUPONT, S., PINZANO, A., MAINARD, D., GALOIS, L., MAGDALOU, J., LOPEZ, E., GILLET, P. & ROUSSEAU, M. (2013) Osteogenic differentiation of human bone marrow mesenchymal stem cells in hydrogel containing nacre powder. *Journal of Biomedical Materials Research Part A,* 101**,** 3211-3218.

FOLK, R. L. (1974) Natural-History of Crystalline Calcium-Carbonate - Effect of Magnesium Content and Salinity. *Journal of Sedimentary Petrology,* 44**,** 40-53.

FOO, L. H., SUZINA, A. H., AZLINA, A. & KANNAN, T. P. (2008) Gene expression analysis of osteoblasts seeded in coral scaffold. *J Biomed Mater Res A,* 87**,** 215-21.

FROST, R. L. (2011) Raman spectroscopic study of the magnesium carbonate mineral hydromagnesite (Mg-5[(CO3)(4)(OH)(2)]center dot 4H(2)O). *Journal of Raman Spectroscopy,* 42**,** 1690-1694.

FROST, R. L., HALES, M. C. & MARTENS, W. N. (2009) Thermogravimetric Analysis of Selected Group (Ii) Carbonateminerals - Implication for the Geosequestration of Greenhouse Gases. *Journal of Thermal Analysis and Calorimetry,* 95**,** 999-1005.

FUJITA, Y., YAMAMURO, T., NAKAMURA, T., KOTANI, S., OHTSUKI, C. & KOKUBO, T. (1991) The bonding behavior of calcite to bone. *J Biomed Mater Res,* 25**,** 991-1003.

GANTAR, A., DA SILVA, L. P., OLIVEIRA, J. M., MARQUES, A. P., CORRELO, V. M., NOVAK, S. & REIS, R. L. (2014) Nanoparticulate bioactive-glass-reinforced gellan-gum hydrogels for bone-tissue engineering. *Mater Sci Eng C Mater Biol Appl,* 43**,** 27-36.

GIAVASIS, I., HARVEY, L. M. & MCNEIL, B. (2000) Gellan gum. *Crit Rev Biotechnol,* 20**,** 177-211.

GKIONI, K., LEEUWENBURGH, S. C., DOUGLAS, T. E., MIKOS, A. G. & JANSEN, J. A. (2010) Mineralization of hydrogels for bone regeneration. *Tissue Eng Part B Rev,* 16**,** 577-85.

GRASSMANN, O. & LOBMANN, P. (2003) Morphogenetic control of calcite crystal growth in sulfonic acid based hydrogels. *Chemistry-a European Journal,* 9**,** 1310-1316.

GRASSMANN, O. & LOBMANN, P. (2004) Biomimetic nucleation and growth of CaCO3 in hydrogels incorporating carboxylate groups. *Biomaterials,* 25**,** 277-282.

GYAWALI, D., NAIR, P., KIM, H. K. & YANG, J. (2013) Citrate-based Biodegradable Injectable hydrogel Composites for Orthopedic Applications. *Biomater Sci,* 1**,** 52-64.

HANCHEN, M., PRIGIOBBE, V., BACIOCCHI, R. & MAZZOTTI, M. (2008) Precipitation in the Mg-carbonate system - effects of temperature and CO2 pressure. *Chemical Engineering Science,* 63**,** 1012-1028.

HELBIG, U. (2008) Growth of calcium carbonate in polyacrylamide hydrogel: Investigation of the influence of polymer content. *Journal of Crystal Growth,* 310**,** 2863-2870.

HOLLINGBERY, L. A. & HULL, T. R. (2010) The thermal decomposition of huntite and hydromagnesite-A review. *Thermochimica Acta,* 509**,** 1-11.

IHLI, J., KULAK, A. N. & MELDRUM, F. C. (2013) Freeze-drying yields stable and pure amorphous calcium carbonate (ACC). *Chemical Communications,* 49**,** 3134-3136.

KOCEN, R., GANTAR, A. & NOVAK, S. (2014) Viscoelastic properties of gellan gum scaffolds with bioactive glass particles. *J Tissue Eng Regen Med,* 8**,** 354-355.

LAMGHARI, M., ALMEIDA, M. J., BERLAND, S., HUET, H., LAURENT, A., MILET, C. & LOPEZ, E. (1999) Stimulation of bone marrow cells and bone formation by nacre: In vivo and in vitro studies. *Bone,* 25**,** 91S-94S.

LAMGHARI, M., ANTONIETTI, P., BERLAND, S., LAURENT, A. & LOPEZ, E. (2001a) Arthrodesis of lumbar spine transverse processes using nacre in rabbit. *Journal of Bone and Mineral Research,* 16**,** 2232-2237.

LAMGHARI, M., BERLAND, S., LAURENT, A., HUET, H. & LOPEZ, E. (2001b) Bone reactions to nacre injected percutaneously into the vertebrae of sheep. *Biomaterials,* 22**,** 555-562.

LANDI, E., LOGROSCINO, G., PROIETTI, L., TAMPIERI, A., SANDRI, M. & SPRIO, S. (2008) Biomimetic Mg-substituted hydroxyapatite: from synthesis to in vivo behaviour. *J Mater Sci Mater Med,* 19**,** 239-47.

LANDI, E., TAMPIERI, A., MATTIOLI-BELMONTE, M., CELOTTI, G., SANDRI, M., GIGANTE, A. & FAVA, P. (2006) Biomimetic Mg- and Mg, CO3-substituted hydroxyapatites: synthesis, characterization and in vitro behaviour. *J Eur Ceram Soc,* 26**,** 2593-601.

LEE, S. K., SILVA-CORREIA, J., CARIDADE, S. G., MANO, J. F., OLIVEIRA, J. M., KHANG, G. & REIS, R. L. (2012) Evaluation of different formulations of gellan gum-based hydrogels for tissue engineering of intervertebral disc. *J Tissue Eng Regen Med,* 6**,** 44-44.

LI, H. & ESTROFF, L. A. (2007) Hydrogels coupled with self-assembled monolayers: an in vitro matrix to study calcite biomineralization. *J Am Chem Soc,* 129**,** 5480-3.

LI, H., XIN, H. L., MULLER, D. A. & ESTROFF, L. A. (2009) Visualizing the 3D internal structure of calcite single crystals grown in agarose hydrogels. *Science,* 326**,** 1244-7.

LIAO, H. H., MUTVEI, H., SJOSTROM, M., HAMMARSTROM, L. & LI, J. G. (2000) Tissue responses to natural aragonite (Margaritifera shell) implants in vivo. *Biomaterials,* 21**,** 457-468.

LONG, X., NASSE, M. J., MA, Y. R. & QI, L. M. (2012) From synthetic to biogenic Mg-containing calcites: a comparative study using FTIR microspectroscopy. *Physical Chemistry Chemical Physics,* 14**,** 2255-2263.

MAEDA, H., MAQUET, V., KASUGA, T., CHEN, Q. Z., ROETHER, J. A. & BOCCACCINI, A. R. (2007) Vaterite deposition on biodegradable polymer foam scaffolds for inducing bone-like hydroxycarbonate apatite coatings. *J Mater Sci Mater Med,* 18**,** 2269-73.

MANDA-GUIBA, M. G., OLIVEIRA, M. B., MANO, J. F., MARQUES, A. P., OLIVEIRA, J. M., CORRELO, V. M. & REIS, R. L. (2012) Gellan gum - hydroxyapatite composite hydrogels for bone tissue engineering. *J Tissue Eng Regen Med,* 6**,** 15-15.

MARTIN, R. I. & BROWN, P. W. (1997) The effects of magnesium on hydroxyapatite formation in vitro from CaHPO4 and Ca4(PO4)2O at 37.4 degrees C. *Calcif Tissue Int,* 60**,** 538-46.

MORRIS, E. R., NISHINARI, K. & RINAUDO, M. (2012) Gelation of gellan - A review. *Food Hydrocolloid,* 28**,** 373-411.

MORSE, J. W., ARVIDSON, R. S. & LUTTGE, A. (2007) Calcium carbonate formation and dissolution. *Chem Rev,* 107**,** 342-81.

MULLER, W. E., SCHRODER, H. C., SCHLOSSMACHER, U., NEUFURTH, M., GEURTSEN, W., KORZHEV, M. & WANG, X. (2013) The enzyme carbonic anhydrase as an integral component of biogenic Ca-carbonate formation in sponge spicules. *FEBS Open Bio,* 3**,** 357-62.

MUNRO, N. H., GREEN, D. W., DANGERFIELD, A. & MCGRATH, K. M. (2011) Biomimetic mineralisation of polymeric scaffolds using a combined soaking and Kitano approach. *Dalton Trans,* 40**,** 9259-68.

MUNRO, N. H. & MCGRATH, K. M. (2012) Biomimetic approach to forming chitin/aragonite composites. *Chem Commun (Camb),* 48**,** 4716-18.

NASH, M. C., OPDYKE, B. N., WU, Z. W., XU, H. F. & TRAFFORD, J. M. (2013) Simple X-Ray Diffraction Techniques to Identify Mg Calcite, Dolomite, and Magnesite in Tropical Coralline Algae and Assess Peak Asymmetry. *Journal of Sedimentary Research,* 83**,** 1085-1099.

OGOMI, D., SERIZAWA, T. & AKASHI, M. (2003) Bioinspired organic-inorganic composite materials prepared by an alternate soaking process as a tissue reconstitution matrix. *J Biomed Mater Res A,* 67**,** 1360-6.

OLIVEIRA, J. T., MARTINS, L., PICCIOCHI, R., MALAFAYA, P. B., SOUSA, R. A., NEVES, N. M., MANO, J. F. & REIS, R. L. (2010) Gellan gum: a new biomaterial for cartilage tissue engineering applications. *J Biomed Mater Res A,* 93**,** 852-63.

PATEL, M., PATEL, K. J., CACCAMESE, J. F., COLETTI, D. P., SAUK, J. J. & FISHER, J. P. (2010) Characterization of cyclic acetal hydroxyapatite nanocomposites for craniofacial tissue engineering. *J Biomed Mater Res A,* 94**,** 408-18.

PAXTON, J. Z., DONNELLY, K., KEATCH, R. P. & BAAR, K. (2009) Engineering the bone-ligament interface using polyethylene glycol diacrylate incorporated with hydroxyapatite. *Tissue Eng Part A,* 15**,** 1201-9.

PHADKE, A., SHIH, Y. R. & VARGHESE, S. (2012) Mineralized synthetic matrices as an instructive microenvironment for osteogenic differentiation of human mesenchymal stem cells. *Macromol Biosci,* 12**,** 1022-32.

PIMENTA, D. R., SILVA-CORREIA, J., CARIDADE, S. G., SOUSA, R. A., OLIVEIRA, J. M., MANO, J. F. & REIS, R. L. (2011) Novel Gellan Gum Hydrogels for Tissue Engineering of Intervertebral Disc. *Int J Artif Organs,* 34**,** 703-703.

RAHMAN, M. A., SHINJO, R., OOMORI, T. & WORHEIDE, G. (2013) Analysis of the Proteinaceous Components of the Organic Matrix of Calcitic Sclerites from the Soft Coral Sinularia sp. *Plos One,* 8.

RAUNER, N., MEURIS, M., DECH, S., GODDE, J. & TILLER, J. C. (2014) Urease-induced calcification of segmented polymer hydrogels - a step towards artificial biomineralization. *Acta Biomater,* 10**,** 3942-51.

RAZ, S., TESTENIERE, O., HECKER, A., WEINER, S. & LUQUET, G. (2002) Stable amorphous calcium carbonate is the main component of the calcium storage structures of the crustacean Orchestia cavimana. *Biological Bulletin,* 203**,** 269-274.

RAZ, S., WEINER, S. & ADDADI, L. (2000) Formation of high-magnesian calcites via an amorphous precursor phase: Possible biological implications. *Advanced Materials,* 12**,** 38-+.

REN, F., LENG, Y., XIN, R. & GE, X. (2010) Synthesis, characterization and ab initio simulation of magnesium-substituted hydroxyapatite. *Acta Biomaterialia,* 6**,** 2787-2796.

RIES, J. B. (2004) Effect of ambient Mg/Ca ratio on Mg fractionation in calcareous marine invertebrates: A record of the oceanic Mg/Ca ratio over the Phanerozoic. *Geology,* 32**,** 981-984.

SANGINARIO, V., GINEBRA, M. P., TANNER, K. E., PLANELL, J. A. & AMBROSIO, L. (2006) Biodegradable and semi-biodegradable composite hydrogels as bone substitutes: morphology and mechanical characterization. *J Mater Sci Mater Med,* 17**,** 447-54.

SATO, M. & MATSUDA, S. (1969) Structure of Vaterite and Infrared Spectra. *Zeitschrift Fur Kristallographie Kristallgeometrie Kristallphysik Kristallchemie,* 129**,** 405-&.

SILVA-CORREIA, J., OLIVEIRA, J. M., CARIDADE, S. G., OLIVEIRA, J. T., SOUSA, R. A., MANO, J. F. & REIS, R. L. (2011) Gellan gum-based hydrogels for intervertebral disc tissue-engineering applications. *J Tissue Eng Regen Med,* 5**,** E97-E107.

SOMMERDIJK, N. A. & DE WITH, G. (2008) Biomimetic CaCO3 mineralization using designer molecules and interfaces. *Chem Rev,* 108**,** 4499-550.

SONG, J., XU, J., FILION, T., SAIZ, E., TOMSIA, A. P., LIAN, J. B., STEIN, G. S., AYERS, D. C. & BERTOZZI, C. R. (2009) Elastomeric high-mineral content hydrogel-hydroxyapatite composites for orthopedic applications. *J Biomed Mater Res A,* 89**,** 1098-107.

STANLEY, S. M., RIES, J. B. & HARDIE, L. A. (2002) Low-magnesium calcite produced by coralline algae in seawater of Late Cretaceous composition. *Proc Natl Acad Sci U S A,* 99**,** 15323-6.

SUZAWA, Y., FUNAKI, T., WATANABE, J., IWAI, S., YURA, Y., NAKANO, T., UMAKOSHI, Y. & AKASHI, M. (2010) Regenerative behavior of biomineral/agarose composite gels as bone grafting materials in rat cranial defects. *J Biomed Mater Res A,* 93**,** 965-75.

SUZUKI, Y., SUZUKI, T. S., SHINODA, Y. & YOSHIDA, K. (2012) Uniformly Porous MgTi2O5 with Narrow Pore-Size Distribution: XAFS Study, Improved In Situ Synthesis, and New In Situ Surface Coating. *Advanced Engineering Materials,* 14**,** 1134-1138.

TRAN, C. T., GARGIULO, C., THAO, H. D., TUAN, H. M., FILGUEIRA, L. & MICHAEL STRONG, D. (2011) Culture and differentiation of osteoblasts on coral scaffold from human bone marrow mesenchymal stem cells. *Cell Tissue Bank,* 12**,** 247-61.

VANDROVCOVA, M., DOUGLAS, T. E. L., MROZ, W., MUSIAL, O., SCHAUBROECK, D., BUDNER, B., SYROKA, R., DUBRUEL, P. & BACAKOVA, L. (2015) Pulsed laser deposition of magnesium-doped calcium phosphate coatings on porous polycaprolactone scaffolds produced by rapid prototyping. *Materials Letters,* 148**,** 178-183.

VIATEAU, V., MANASSERO, M., SENSEBE, L., LANGONNE, A., MARCHAT, D., LOGEART-AVRAMOGLOU, D., PETITE, H. & BENSIDHOUM, M. (2013) Comparative study of the osteogenic ability of four different ceramic constructs in an ectopic large animal model. *J Tissue Eng Regen Med*.

WEBSTER, T. J., ERGUN, C., DOREMUS, R. H. & BIZIOS, R. (2002) Hydroxylapatite with substituted magnesium, zinc, cadmium, and yttrium. II. Mechanisms of osteoblast adhesion. *J Biomed Mater Res,* 59**,** 312-7.

WHITE, W. B. (1971) Infrared Characterization of Water and Hydroxyl Ion in Basic Magnesium Carbonate Minerals. *American Mineralogist,* 56**,** 46-&.

XIE, M., OLDEROY, M. O., ANDREASSEN, J. P., SELBACH, S. M., STRAND, B. L. & SIKORSKI, P. (2010) Alginate-controlled formation of nanoscale calcium carbonate and hydroxyapatite mineral phase within hydrogel networks. *Acta Biomater,* 6**,** 3665-75.

XUE, W., DAHLQUIST, K., BANERJEE, A., BANDYOPADHYAY, A. & BOSE, S. (2008) Synthesis and characterization of tricalcium phosphate with Zn and Mg based dopants. *J Mater Sci Mater Med,* 19**,** 2669-77.

XYLA, A. G. & KOUTSOUKOS, P. G. (1989) Quantitative-Analysis of Calcium-Carbonate Polymorphs by Infrared-Spectroscopy. *Journal of the Chemical Society-Faraday Transactions I,* 85**,** 3165-3172.

YAMASAKI, Y., YOSHIDA, Y., OKAZAKI, M., SHIMAZU, A., KUBO, T., AKAGAWA, Y. & UCHIDA, T. (2003) Action of FGMgCO3Ap-collagen composite in promoting bone formation. *Biomaterials,* 24**,** 4913-20.

YAMASAKI, Y., YOSHIDA, Y., OKAZAKI, M., SHIMAZU, A., UCHIDA, T., KUBO, T., AKAGAWA, Y., HAMADA, Y., TAKAHASHI, J. & MATSUURA, N. (2002) Synthesis of functionally graded MgCO3 apatite accelerating osteoblast adhesion. *J Biomed Mater Res,* 62**,** 99-105.

ZHANG, J., MA, X. Y., LIN, D., SHI, H. S., YUAN, Y., TANG, W., ZHOU, H. J., GUO, H., QIAN, J. C. & LIU, C. S. (2015) Magnesium modification of a calcium phosphate cement alters bone marrow stromal cell behavior via an integrin-mediated mechanism. *Biomaterials,* 53**,** 251-264.

ZHAO, S. F., JIANG, Q. H., PEEL, S., WANG, X. X. & HE, F. M. (2012) Effects of magnesium-substituted nanohydroxyapatite coating on implant osseointegration. *Clin Oral Implants Res*.

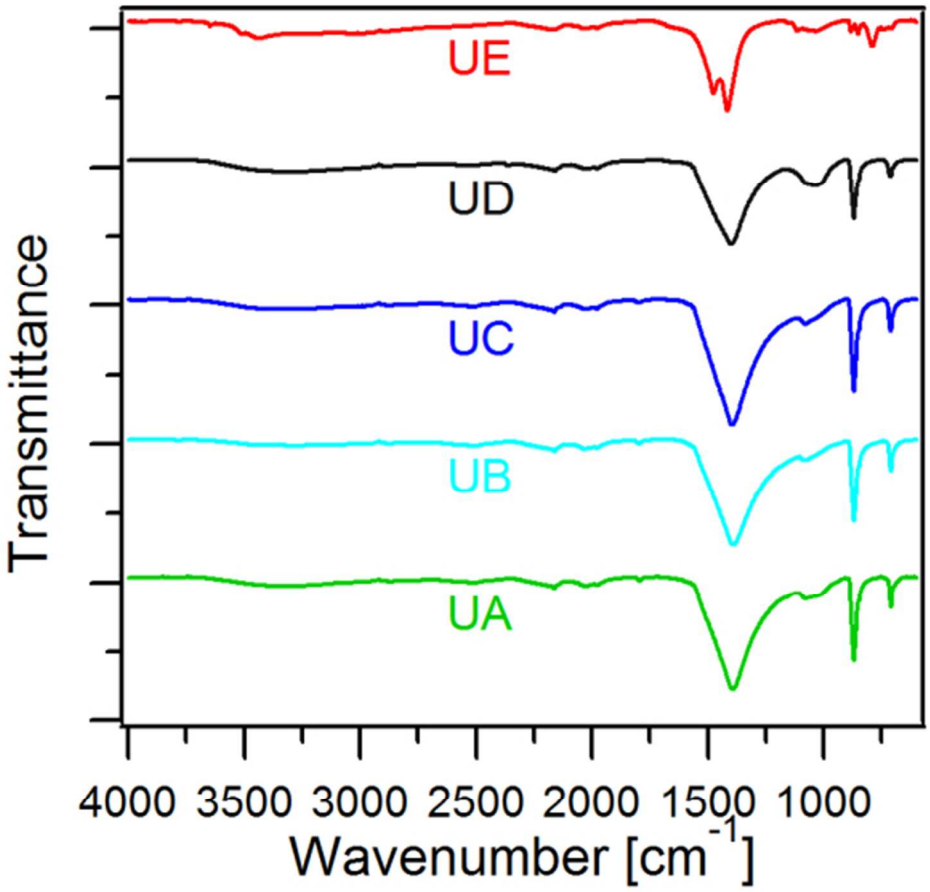

Figure 1. FTIR spectra in the wavelength range 600-4000 cm-1 of GG hydrogels preincubated in 50 mg/ml urease and subsequently incubated for 5 days in mineralization media UA, UB, UC, UD and UE. Bands characteristic for calcite in sample groups UA, UB, UC and UD are visible at 1400, 871 and 712 cm-1. Bands characteristic for hydromagnesite in sample group UE are visible at 1478, 1416, 792, 744 and 714 cm-1. A shoulder characteristic for hydromagnesite is visible at 1646 cm-1.
Figure 1
52x48mm (300 x 300 DPI)

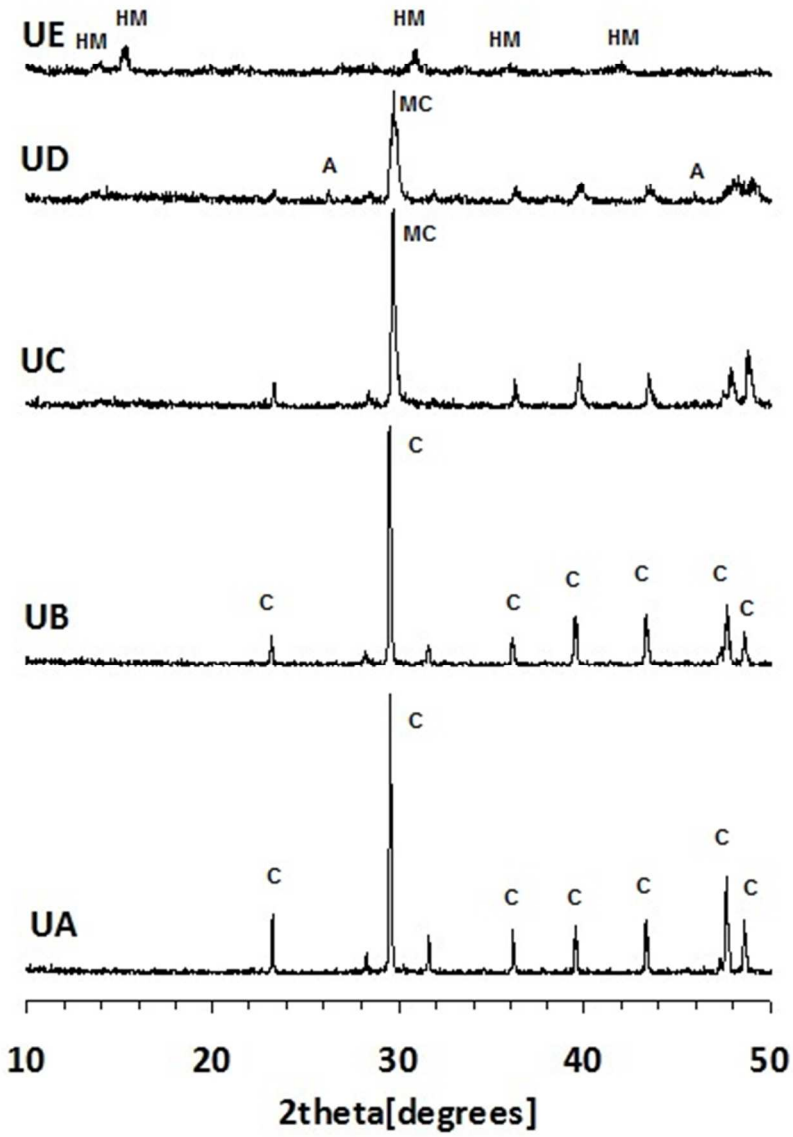

Figure 2. XRD diffractograms of GG hydrogels preincubated in 50 mg/ml urease and subsequently incubated for 5 days in mineralization media UA, UB, UC, UD or UE. C: calcite; MC: magnesian calcite; A: aragonite; HM: hydromagnesite.

36x53mm (300 x 300 DPI)

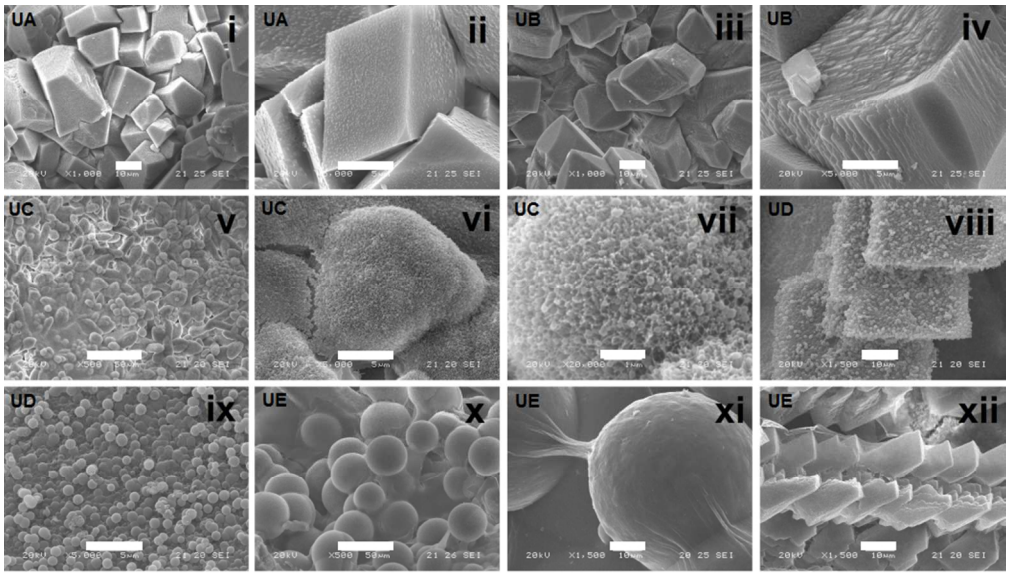

Figure 3. SEM micrographs of GG hydrogels preincubated in 50 mg/ml urease and subsequently incubated for 5 days in mineralization media UA, UB, UC, UD or UE. i, ii: UA; iii, iv: UB; v, vi, vii: UC; viii, ix: UD; x, xi, xii: UE. Scale bars: i: 10 μm; ii: 5 μm; iii: 10 μm; iv: 5 μm; v: 50 μm; vi: 5 μm; vii: 1 μm; viii: 10 μm; ix: 5 μm; x: 50 μm; xi: 10 μm; xii: 5 μm. The scale bars are indicated on each figure.

88x50mm (300 x 300 DPI)

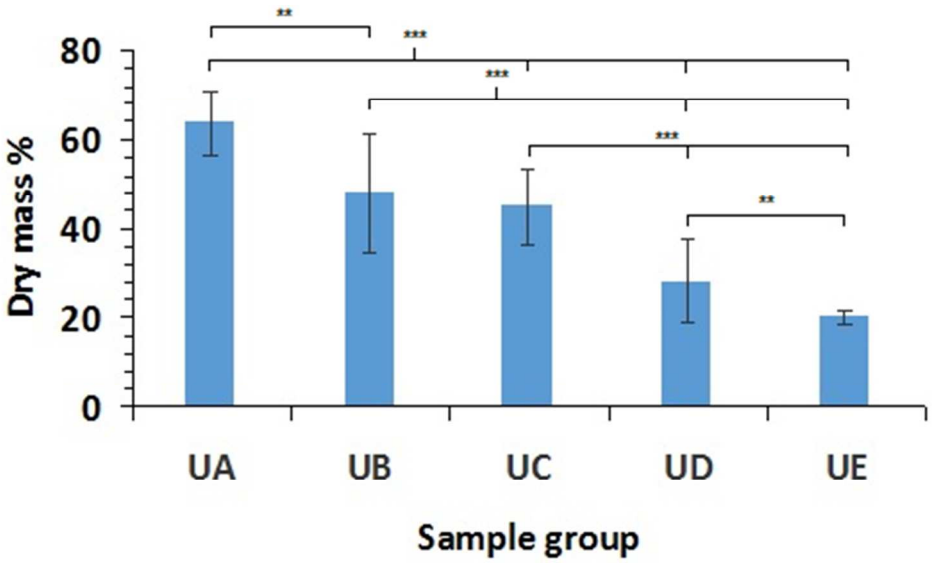

Figure 4. Dry mass percentage of GG hydrogels preincubated in 50 mg/ml urease and subsequently incubated for 5 days in mineralization media UA, UB, UC, UD or UE. Error bars show standard deviation.

135x77mm (96 x 96 DPI)

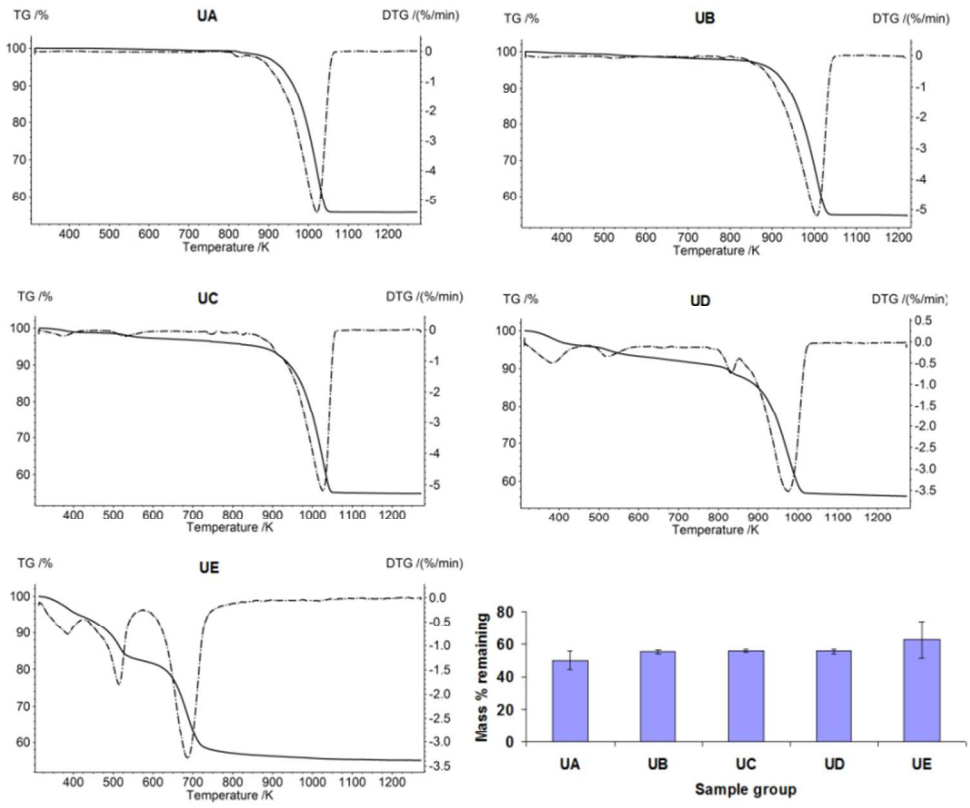

Figure 5. Thermogravimetric analysis of GG hydrogels preincubated in 50 mg/ml urease and subsequently incubated for 5 days in mineralization media UA, UB, UC, UD or UE. Representative graphs showing residual mass percentage (TG) and rate of change of TG (DTG) are shown for each sample group. Bottom right: residual mass percentage after heating to 1273 K. Error bars show standard deviations. No statistically significant differences were observed.

Figure 5

76x64mm (300 x 300 DPI)

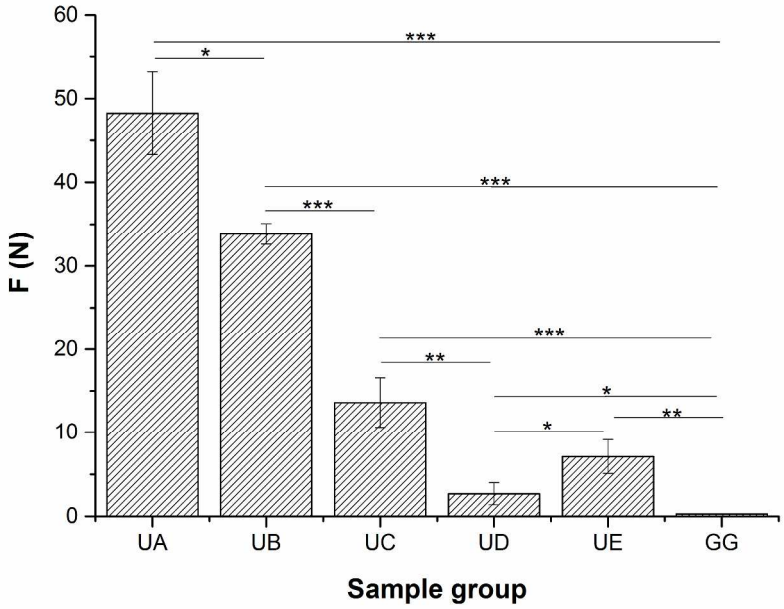

Figure 6. Compressive testing of GG hydrogels preincubated in 50 mg/ml urease and subsequently incubated for 5 days in mineralization media UA, UB, UC, UD or UE. y-axis: force required to compress samples by 80%. Error bars show standard deviation.

288x201mm (300 x 300 DPI)

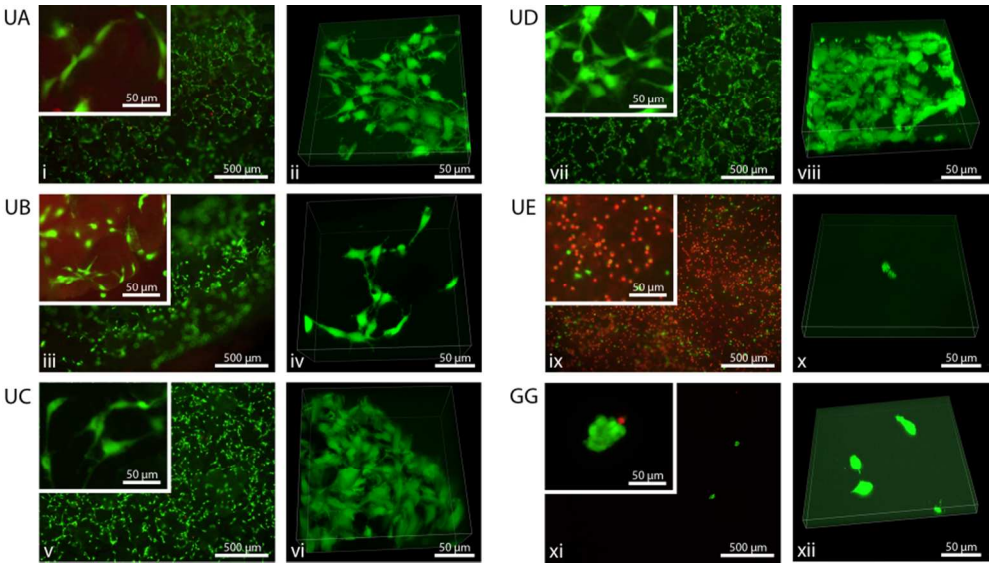

Figure 7. Fluorescence and Confocal Laser Scanning microscopy images of MC3T3-E1 osteoblast-like cells cultivated for 1 day and 7 days on GG hydrogels preincubated in 50 mg/ml urease and subsequently incubated for 5 days in mineralization media UA, UB, UC, UD or UE. Fluorescence microscopy (i, iii, v, vii, ix, xi and inserts) evaluation of cells seeded at a high concentration (cell adhesion test) on GG hydrogels after 1 day. Confocal laser scanning microscopy (ii, iv, vi, viii, x, xii) evaluation of cells seeded at a low concentration (cell proliferation test) on GG hydrogels after 7 days.
i, ii: UA, 1 and 7 days respectively; iii, iv: UB, 1 and 7 days respectively; v, vi: UC: 1 and 7 days respectively; vii, viii: UD: 1 and 7 days respectively; ix, x: UE: 1 and 7 days respectively; xi, xii: GG: 1 and 7 days respectively.

88x49mm (300 x 300 DPI)

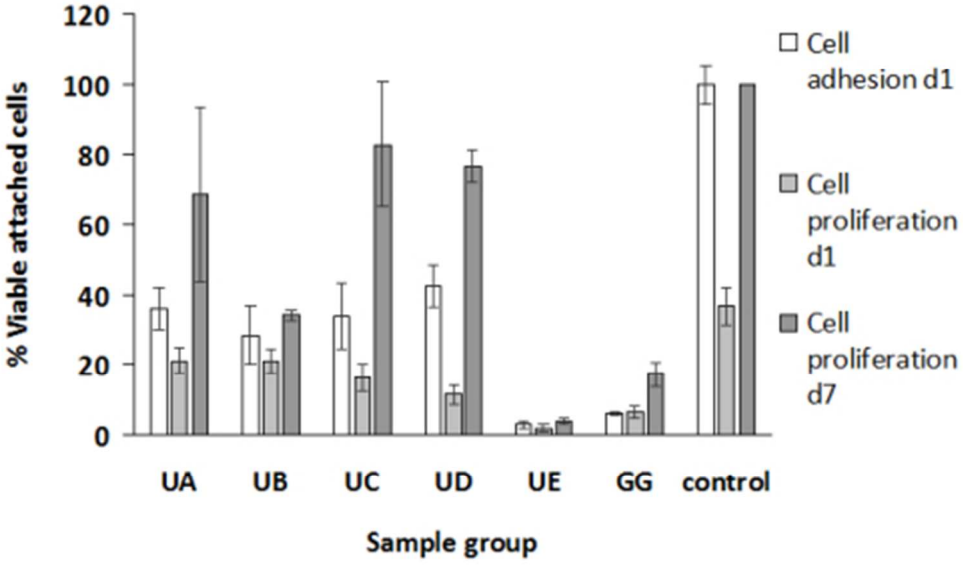

Figure 8. Percentage of viable attached cells on GG hydrogels preincubated in 50 mg/ml urease and subsequently incubated for 5 days in mineralization media UA, UB, UC, UD or UE. Cells were seeded and evaluated after 1 day (cell adhesion) respectively 1 and 7 days (cell proliferation). The amount of viable cells was quantified using the MTT assay by calculating relative to the control (tissue culture polystyrene) of day 1 (cell adhesion) or day 7 (cell proliferation).

42x25mm (300 x 300 DPI)